Supporting Information

Branching effect on the linear and nonlinear optical properties of styrylpyrimidines

Fotis Kournoutas,[a] Arnaud Fihey,[b] Jean-Pierre Malval,[c] Arnaud Spangenberg,[c] Michaela Fecková,[b,d] Pascal le Poul,[b] Claudine Katan,[b] Françoise Robin-le Guen,[b] Filip Bureš,[d] Sylvain Achelle[b,*], Mihalis Fakis[a,*]

[a]Department of Physics, University of Patras, Greece, GR-26504 Patras, Greece.

[b]Univ Rennes, CNRS, ISCR (Institut des Sciences Chimiques de Rennes) - UMR 6226, F 35000 Rennes, France.

[c]Institut de Science des Matériaux de Mulhouse CNRS-UMR 7361, Université de Haute Alsace, 15 rue Jean Starcky, 68057, Mulhouse, France.

[d]Institute of Organic Chemistry and Technology, Faculty of Chemical Technology, University of Pardubice, Studenská 573, Pardubice 53210, Czech Republic.

Formulation for the calculation of the dipole moments

The transition dipole moment of absorption for the compounds were determined for CH_2Cl_2 through the equation[S1]

$$\mu_{abs} = 9.854 \times 10^{-2} \left[\frac{1}{n[f(n)]^2} \frac{1}{\int_{S1}} \frac{\epsilon(v)}{v} dv \right]^{1/2}$$

where n is the refractive index of the solvent, $f(n) = 3n/(2n^2 + 1)$ and $\epsilon(v)$ is the molar extinction coefficient.

The emission transition dipole moment, is calculated by means of the equation[S1]

$$\mu_{em} = 1785.7 \left[\frac{\Phi}{\tau_F n^3 [f(n)]^2 \tilde{\nu}_f^3} \right]^{1/2}$$

where Φ is the fluorescence quantum yield, τ_F the fluorescence lifetime, n the solvent refractive index, $f(n) = 3n/(2n^2 + 1)$ and $\tilde{\nu}_f^3$ is the average cubic fluorescence frequency expressed by:

$$\tilde{\nu}_f^3 = \frac{\int I(v) dv}{\int I(v) / v^3 dv}$$

The fluorescence quantum yields in CH_2Cl_2 were 0.15, 0.45, 0.4, 0.55, 0.22 and 0.56 for **1a**, **2a**, **1b**, **2b**, **1c** and **2c** respectively.

S1 Lewis, J.E.; Maroncelli, M. On the (Uninteresting) Dependence of the Absorption and Emission Transition Moments of Coumarin 153 on Solvent. *Chem. Phys. Lett.*, **1998**, *282*, 197-203.

Sample	Solvent	λ_{abs} (nm)	λ_{em} (nm)
1a	n-HEX	373	408
	TOL	386	452
	THF	388	480
	$CHCl_3$	396	484
	CH_2Cl_2	392	493
	ACT	387	502
	ACN	388	512
2a	n-HEX	388	425
	TOL	395	468
	THF	395	503
	$CHCl_3$	409	522
	CH_2Cl_2	399	531
	ACT	391	537
	ACN	392	557
1b	n-HEX	398	430
	TOL	415	475
	THF	420	520
	$CHCl_3$	428	526
	CH_2Cl_2	426	526
	ACT	423	564
	ACN	424	589
2b	n-HEX	408	443
	TOL	427	475
	THF	424	518
	$CHCl_3$	435	541
	CH_2Cl_2	430	538
	ACT	420	565
	ACN	421	598
1c	n-HEX	379	430
	TOL	395	468
	THF	395	515
	$CHCl_3$	401	515
	CH_2Cl_2	403	519
	ACT	398	555
	ACN	400	580
2c	n-HEX	405	444
	TOL	413	473
	THF	409	514
	$CHCl_3$	417	527
	CH_2Cl_2	415	531
	ACT	408	553
	ACN	407	585

Table S1. Photophysical properties of **1a-1c** and **2a-2c** in various solvents.

Solvent	ε	$f(\varepsilon)$
n-HEX	1.89	0.186
TOL	2.38	0.239
$CHCl_3$	4.81	0.359
THF	7.58	0.407
CH_2Cl_2	8.93	0.420
ACT	20.70	0.464
DMF	37.50	0.480
ACN	36.71	0.480

Table S2. Solvent parameters. ε: dielectric constant, $f(\varepsilon)$ the low-frequency polarizabilities.

Sample	Solvent	A_1	τ_1 (ns)	A_2	τ_2 (ns)	A_3	τ_3 (ns)	$\langle\tau\rangle$ (ns)
1a	n-Hex	99.1%	0.02	0.8%	0.20			0.03
	TOL	99.8%	0.07	0.2%	1.30	-	-	0.07
	THF	24%	0.06	76%	0.17	-	-	0.15
	$CHCl_3$	16%	0.06	84%	0.13	-	-	0.11
	CH_2Cl_2	33%	0.07	67%	0.20	-	-	0.16
	ACT	41%	0.20	59%	0.38	-	-	0.31
	ACN	31%	0.18	69%	0.51	-	-	0.41
2a	n-Hex	80%	0.78	20%	1.18	-	-	0.86
	TOL	100%	1.36	-	-	-	-	1.36
	THF	100%	2.54	-	-	-	-	2.54
	$CHCl_3$	100%	2.39	-	-	-	-	2.39
	CH_2Cl_2	100%	3.11	-	-	-	-	3.11
	ACT	100%	3.18	-	-	-	-	3.18
	ACN	65%	2.73	35%	3.21	-	-	2.88
1b	n-Hex	100%	0.41	-	-	-	-	0.41
	TOL	31%	0.46	69%	0.93	-	-	0.79
	THF	12%	0.52	88%	1.96	-	-	1.79
	$CHCl_3$	23%	0.42	77%	1.67	-	-	1.37
	CH_2Cl_2	13%	0.84	87%	2.11	-	-	1.95
	ACT	32%	0.91	68%	2.18	-	-	1.78
	ACN	31%	0.40	69%	1.48	-	-	1.14
2b	n-Hex	100%	1.14	-	-	-	-	1.14
	TOL	22%	0.88	78%	1.55	-	-	1.40
	THF	100%	2.43	-	-	-	-	2.43
	$CHCl_3$	16%	0.40	84%	2.42	-	-	2.10
	CH_2Cl_2	100%	2.87	-	-	-	-	2.87
	ACT	13%	1.18	87%	2.72	-	-	2.53
	ACN	48%	0.86	52%	1.81	-	-	1.35
1c	n-Hex	100%	0.71	-	-	-	-	0.71
	TOL	37%	0.56	63%	1.25	-	-	0.99
	THF	75%	0.10	25%	2.76	-	-	0.75
	$CHCl_3$	36%	0.5	64%	2.18			1.58
	CH_2Cl_2	16%	1.06	84%	2.98			2.68
	ACT	76%	0.23	23%	0.69	1%	2.18	0.36
	ACN	98%	0.30	2%	1.6	-	-	0.33
2c	n-Hex	100%	1.26	-	-	-	-	1.26
	TOL	45%	1.21	55%	1.66	-	-	1.46
	THF	22%	0.19	78%	2.72			2.18
	$CHCl_3$	19%	0.50	81%	2.47	-	-	2.10
	CH_2Cl_2	10%	1.26	90%	3.23	-	-	3.04
	ACT	47%	0.22	28%	1.82	25%	2.66	1.27
	ACN	44%	0.36	55%	1.1	1%	2.83	0.80

Table S3. Fitting parameters for the ns fluorescence dynamics of the herein studied compounds.

Wavelength (nm)	A_1	τ_1 (ps)	A_2	τ_2 (ps)
430	0.20	0.82	0.34	7.4
440	0.17		0.30	
450	0.18		0.25	
460	0.13		0.13	
470	0.05		0.07	
480	0.02		-0.01	
490	-0.07		-0.05	
500	-0.10		-0.12	
510	-0.11		-0.15	
520	-0.06		-0.1	
530	-0.07		-0.18	
540	-0.17		-0.19	

Table S4. Fitting parameters of the FU dynamics for **2a** in TOL after a global fitting analysis.

Wavelength (nm)	A_1	τ_1 (ps)	A_2	τ_2 (ps)
460	0.89	0.82	0.11	3.34
470	0.92		0.08	
480	0.90		0.10	
490	0.80		0.12	
500	0.70		0.22	
510	0.54		0.21	
520	0.29		0.28	
530	0.12		0.30	
540	-0.03		0.23	
550	-0.05		0.16	
560	-0.29		0.17	
570	-0.32		0.06	
580	-0.32		0.01	
590	-0.44		0.01	
600	-0.71		-0.04	
610	-0.44		-0.05	
620	-0.40		-0.11	
630	-0.23		-0.17	

Table S5. Fitting parameters of the FU dynamics for **2a** in ACT after a global fitting analysis.

Wavelength (nm)	A_1	τ_1 (ps)	A_2	τ_2 (ps)
440	0.56	1.08	0.20	7.00
450	0.31		0.34	
460	0.19		0.40	
470	-0.01		0.36	
480	-0.04		0.27	
490	-0.03		0.01	
500	-0.08		-0.01	
510	-0.12		-0.03	
520	-0.16		-0.12	
530	-0.13		-0.14	
540	-0.10		-0.21	
550	-0.09		-0.20	
560	-0.15		-0.20	
570	-0.14		-0.23	

Table S6. Fitting parameters of the FU dynamics for **2b** in TOL after a global fitting analysis.

Wavelength (nm)	A_1	τ_1 (ps)	A_2	τ_2 (ps)
480	0.77	0.39	0.20	1.56
490	0.72		0.25	
500	0.70		0.27	
510	0.46		0.60	
520	0.51		0.44	
530	0.21		0.7	
540	0.19		0.63	
550	-0.08		0.54	
560	-0.29		0.32	
570	-0.24		0.35	
580	-0.19		0.20	
590	-0.05		-0.004	
600	-0.06		-0.08	
610	-0.09		-0.19	
620	-0.12		-0.27	
630	-0.08		-0.38	
640	-0.15		-0.24	
650	-0.26		-0.20	

Table S7. Fitting parameters of the FU dynamics for **2b** in ACT after a global fitting analysis.

Wavelength (nm)	A_1	τ_1 (ps)	A_2	τ_2 (ps)
440	0.57	0.65	0.33	5.61
450	0.27		0.38	
460	0.15		0.31	
470	0.04		0.19	
480	-0.01		0.10	
490	-0.05		-0.03	
500	-0.20		-0.01	
510	-0.10		-0.09	
520	-0.03		-0.16	
530	-0.06		-0.19	
540	-0.01		-0.23	
550	-0.07		-0.21	
560	-0.07		-0.24	
570	-0.16		-0.25	

Table S8. Fitting parameters of the FU dynamics for **2c** in TOL after a global fitting analysis.

Wavelength (nm)	A_1	τ_1 (ps)	A_2	τ_2 (ps)
480	0.89	0.39	0.11	1.56
490	0.81		0.19	
500	0.78		0.22	
510	0.42		0.58	
520	0.52		0.48	
530	0.19		0.63	
540	0.16		0.59	
550	-0.08		0.54	
560	-0.19		0.32	
570	-0.24		0.35	
580	-0.19		0.20	
590	-0.05		-0.01	
600	-0.06		-0.08	
610	-0.04		-0.19	
620	-0.02		-0.27	
630	-0.04		-0.39	
640	-0.05		-0.24	
650	-0.07		-0.20	

Table S9. Fitting parameters of the FU dynamics for **2c** in ACT after a global fitting analysis.

Compound	GS	ES	Difference
1a	0.1043	0.0184	-0.0859
2a	0.1058	0.0349	-0.0709
1b			
branch 1	0.1053	0.0580	-0.0473
branch 2	0.1053	0.0580	-0.0473
2b			
branch 1	0.1080	0.0651	-0.0429
branch 2	0.1080	0.0651	-0.0429
1c			
branch 1	0.1125	0.1220	+0.0095
branch 2	0.1078	0.0723	-0.0355
branch 3	0.1086	0.0482	-0.0604
2c			
branch 1	0.1144	0.1273	+0.0129
branch 2	0.1096	0.0937	-0.0159
branch 3	0.1104	0.0416	-0.0688

Table S10. Bond length alternation (BLA), computed for the vinylene moieties of Confo1 (Figure S8) at the PBE0/6-31G(d,p) (GS) and CAM-B3LYP/6-31G(d,p) (ES) levels of theory.

Compound	Absorption: λ_{abs} (nm)/*f* (orbitals contributions)		Emission: λ_{em} (nm)/*f*	
	PBE0	CAM-B3LYP	PBE0	CAM-B3LYP
1a	357 / 1.05 (HOMO->LUMO)	326 / 1.17 (HOMO->LUMO)	376 / 1.11	363 / 1.22
2a	402 / 0.93 (HOMO->LUMO)	348 / 1.20 (HOMO->LUMO)	538 / 0.07	387 / 1.21
1b Confo1	403 / 1.60 (HOMO->LUMO) 316 / 0.79 (HOMO-1->LUMO+1)	351 / 2.24 (HOMO->LUMO) 313 / 0.14 (HOMO-1->LUMO)	427 / 1.65	377 / 2.27
1b Confo2	390 / 1.09 (HOMO->LUMO) 343 / 0.58 (HOMO->LUMO+1) 329 / 0.37 (HOMO-1->LUMO) (HOMO->LUMO+1)	344 / 1.67 (HOMO->LUMO) 305 / 0.57 (HOMO-1->LUMO) (HOMO->LUMO+1)	421 / 1.11	373 / 1.66
2b Confo1	442 / 1.71 (HOMO->LUMO) 346 / 0.51 (HOMO-1->LUMO+1)	370 / 2.49 (HOMO->LUMO) 335 / 0.16 (HOMO-1->LUMO) (HOMO->LUMO+1)	481 / 1.47	396 / 2.54
2b Confo2	428 / 1.34 (HOMO->LUMO) 393 / 0.22 (HOMO-1->LUMO) 371 / 0.30 (HOMO-1->LUMO+1) 366 / 0.16 (HOMO->LUMO+1)	364 / 1.89 (HOMO->LUMO) 331 / 0.53 (HOMO-1->LUMO) (HOMO->LUMO+1)	471 / 1.15	390 / 1.92
1c Confo1	416 / 0.43 (HOMO->LUMO) 389 / 1.11 (HOMO-1->LUMO) 374 / 0.66 (HOMO-2->LUMO) (HOMO->LUMO+1) 342 / 0.40 (HOMO-2->LUMO+1) (HOMO-1->LUMO+1)	351 / 1.81 (HOMO->LUMO) 331 / 1.33 (HOMO-2->LUMO) (HOMO->LUMO+1) 308 / 0.34 (HOMO-1->LUMO) (HOMO->LUMO)	504 / 0.05	378 / 1.90
1c Confo2	405 / 0.27 (HOMO->LUMO) 376 / 1.27 (HOMO-1->LUMO) (HOMO->LUMO+1) 373 /0.80 (HOMO-1->LUMO) (HOMO->LUMO+1) 358/ 0.29 (HOMO-2->LUMO+1) (HOMO-2->LUMO) (HOMO-1->LUMO+1)	344 / 1.34 (HOMO->LUMO) (HOMO-1->LUMO) 329 / 2.09 (HOMO->LUMO+1) 306 / 0.29 (HOMO-2->LUMO+1) (HOMO->LUMO)	490 / 0.06	374 / 1.38

1c Confo3	410 / 0.39 (HOMO->LUMO) 382 / 0.76 (HOMO-1->LUMO) 371 / 1.19 (HOMO-2->LUMO) (HOMO->LUMO+1) 350 / 0.55 (HOMO-1->LUMO+1)	347 / 1.67 (HOMO->LUMO+1) 329 / 1.70 (HOMO->LUMO+1) (HOMO-2->LUMO) 307 / 0.36 (HOMO-1->LUMO) (HOMO->LUMO)	500 / 0.07	377 / 1.68
2c Confo1	444 / 0.97 (HOMO->LUMO) 428 / 0.75 (HOMO-1->LUMO) 414 / 0.68 (HOMO-2->LUMO) 380 / 0.42 (HOMO->LUMO+1) (HOMO-2->LUMO) (HOMO-1->LUMO+1)	369 / 2.26 (HOMO->LUMO) (HOMO-1->LUMO) 353 / 1.41 (HOMO-2->LUMO) (HOMO->LUMO+1) 322 / 0.14 (HOMO-2->LUMO) (HOMO->LUMO+1)	536 / 0.06	400 / 2.17
2c Confo2	431 / 0.65 (HOMO->LUMO) 418 / 1.33 (HOMO-1->LUMO) (HOMO->LUMO+1) 410 / 0.76 (HOMO->LUMO+1) (HOMO-1->LUMO)	363 / 1.73 (HOMO-1->LUMO) (HOMO->LUMO) (HOMO-2->LUMO+1) 352 / 2.14 (HOMO->LUMO+1) (HOMO->LUMO+2)	525 / 0.07	395 / 1.72
2c Confo 3	437 / 0.87 (HOMO->LUMO) (HOMO-1->LUMO) 420 / 0.65 (HOMO-1->LUMO) (HOMO->LUMO) 412 / 1.12 (HOMO-2->LUMO) (HOMO->LUMO+1) 384 / 0.28 (HOMO-2->LUMO) (HOMO-1->LUMO+1)	365 / 2.09 (HOMO->LUMO) (HOMO-1->LUMO) 352 / 1.77 (HOMO-2->LUMO) (HOMO->LUMO+1)	535 / 0.07	396 / 2.06

Table S11. Absorption and emission properties of **1a-c** and **2a-c** considering the conformers depicted in Figure S8. *f* corresponds to the oscillator strength. All ground-state geometries are obtained at the PBE0/6-31G(d,p) level of theory while the vertical absorption and emission properties are obtained at the PBE0/6-31G(d,p) or CAM-B3LYP/6-31G(d,p) level.

		i	μ_{00} (D)	μ_{ii} (D)	$\Delta\mu$ (D)	μ_{0i} (D)	σ_2 [two states] (GM)
2a	B3LYP 6-31G(d)	1	4.55	18.02	13.47	8.70	158
	CAM-B3LYP 6-31G(d,p)	1	4.10	13.32	9.22	9.43	87
2b	B3LYP 6-31G(d)	1	3.25	7.08	3.83	12.21	25
		2	3.25	7.30	4.05	2.45	1
	CAM-B3LYP 6-31G(d,p)	1	3.01	5.75	2.74	14.00	17
		2	3.01	5.73	2.72	3.40	1

Table S12. Computed state dipole moments, difference and transition dipole moments relevant to vertical absorption of **2a-b** considering the conformers depicted in Figure S8. 2PA cross section computed within a two-state model using the dipole moments.[i] i=1 and 2 provide information relevant to the S_0-S_1 and S_0-S_2 transition, respectively.

μ^{x}_{0i} (D)		μ^{x}_{0i} (D)	μ^{y}_{0i} (D)	μ^{z}_{0i} (D)
1b	S_0-S_1	12.94	0.00	0.03
	S_0-S_2	0.00	3.08	0.00
2b	S_0-S_1	14.00	0.00	0.10
	S_0-S_2	0.00	3.41	0.00

Table S13. Transition dipole moment components computed for the ground state geometry (relevant to absorption) at the CAM-B3LYP/6-31G(d,p) level of theory

Sample	$\frac{\partial \nu^{ST}}{\partial F}$ (eV)	a (Å)	δ^{MAX} (GM)	μ_{abs} (D)
1b	1.84	5.2	27	8.3
1c	1.81	5.2	43	10.3
2b	1.80	5.8	64	9.07
2c	2.01	5.8	86	9.27

Table S14. Data used for the correlation between $\frac{\delta^{\max}}{\mu_{abs}^2}$ and $\frac{\partial \nu^{ST}}{\partial F}.a^3$ parameters

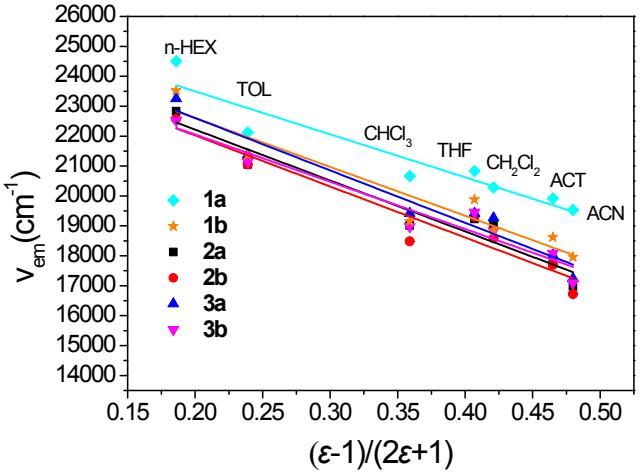

Figure S1. Plot of the solvent shift of the fluorescence peak of the studied compounds as a function of $f(\varepsilon) = (\varepsilon - 1)/(2\varepsilon + 1)$.

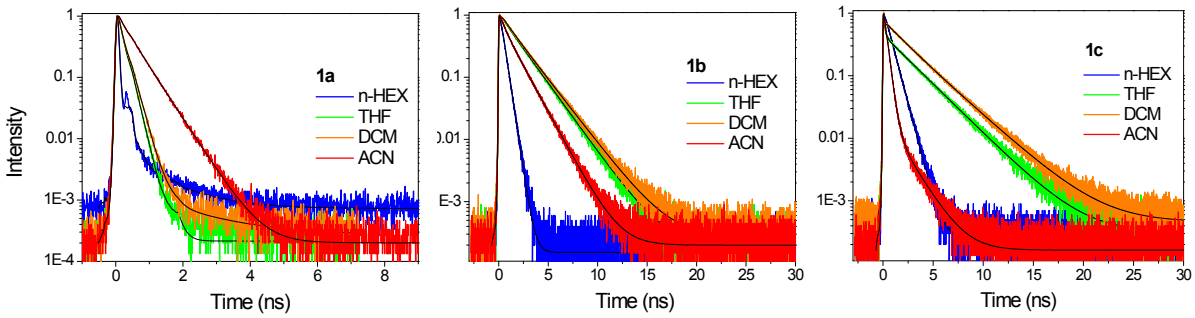

Figure S2. Nanosecond fluorescence dynamics of compounds **1a**, **1b** and **1c** in various solvents.

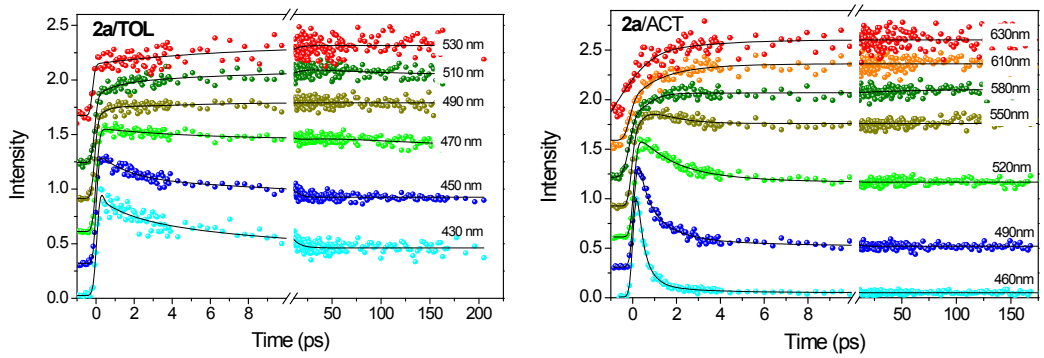

Figure S3. Femtosecond time resolved upconversion dynamics of **2a** in TOL and ACT. The transients have been shifted for clarity.

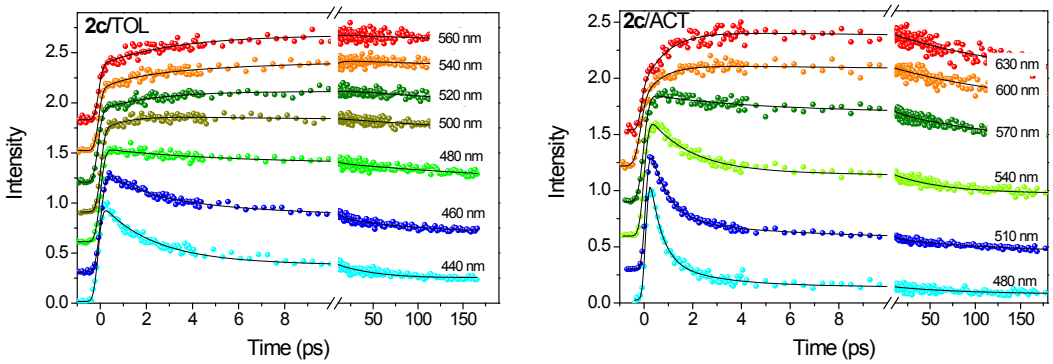

Figure S4. Femtosecond time resolved upconversion dynamics of **2c** in TOL and ACT. The transients have been shifted for clarity.

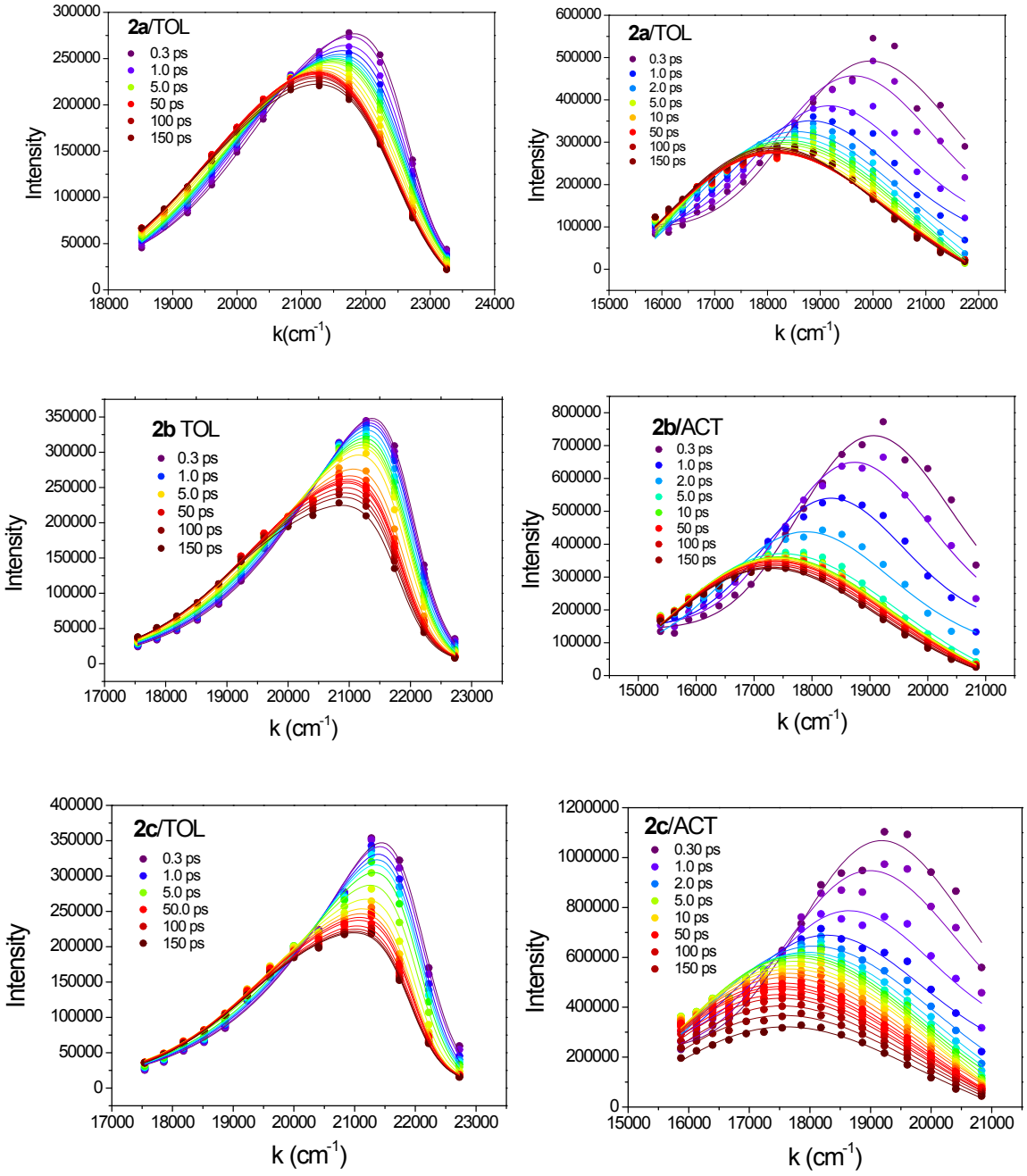

Figure S5. TRES for **2a**, **2b**, **2c** in TOL and ACT and fitting functions. The insets show some characteristic times.

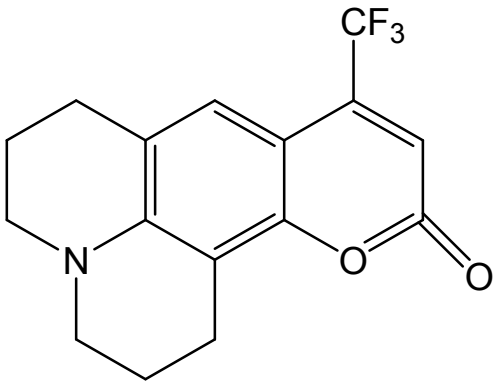

Figure S6. The chemical structure of Coumarin 153.

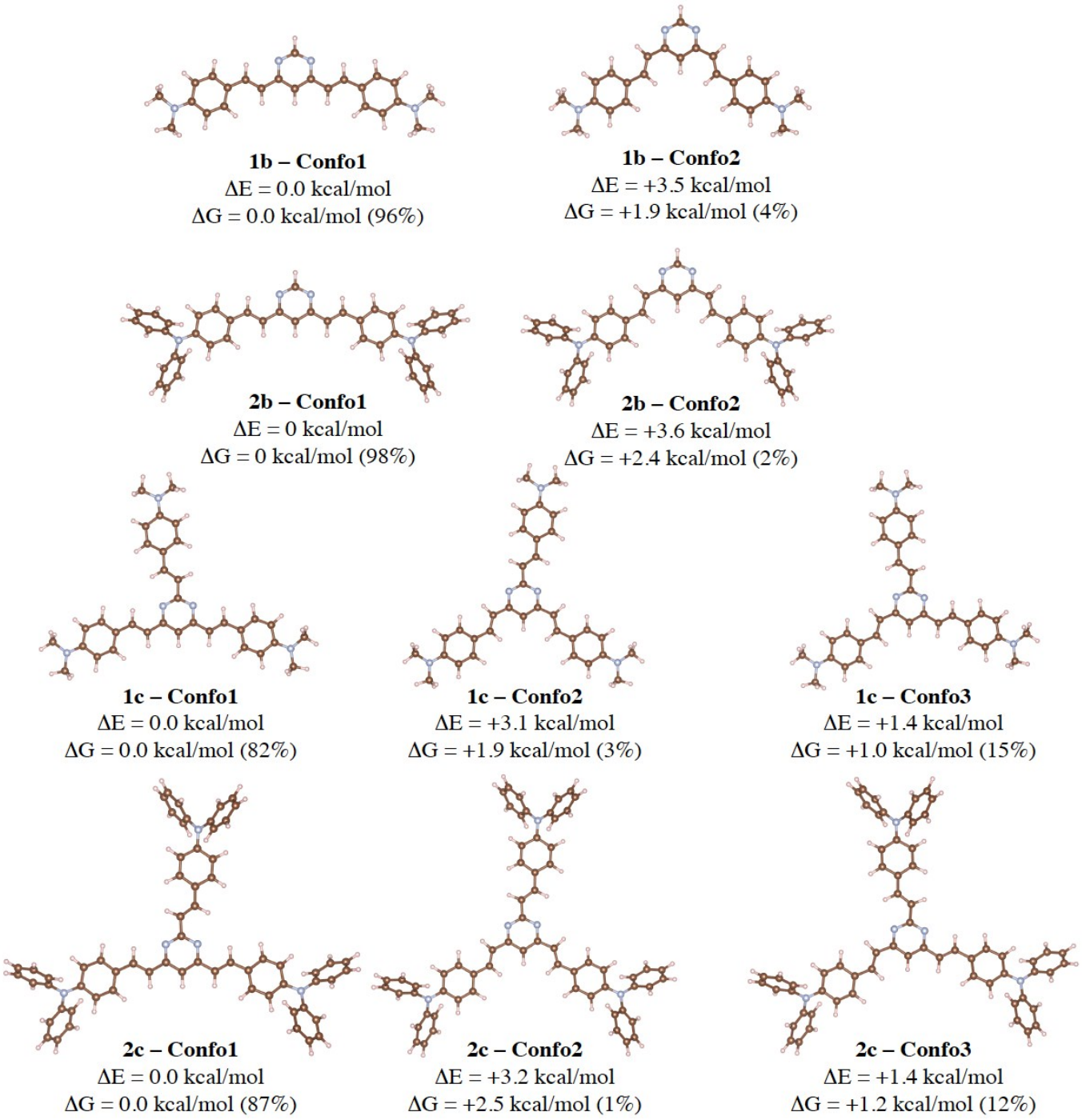

Figure S7. Relative stability of the different conformers (PBE0/6-31G(d,p)). Both electronic energy difference (ΔE) and free energy difference (ΔG) are given. The most stable conformer (Confo1) is taken as a reference for the energy differences, and in parenthesis are given the corresponding Boltzmann distribution, in percentages.

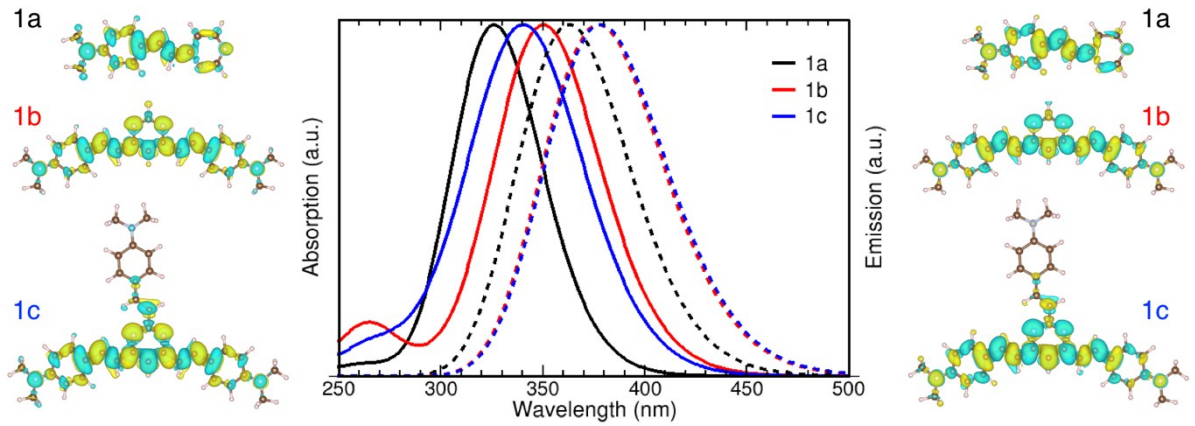

Figure S8. Computed optical properties of **1a-c** in vacuum (For **2a-c** see Figure 1). The central panel shows in arbitrary units normalized absorption (full lines) and emission spectra (dashed lines). Transition densities of the lowest lying excited state relevant to absorption and emission are depicted on the left and right sides. See the main text for details on the computational protocol.

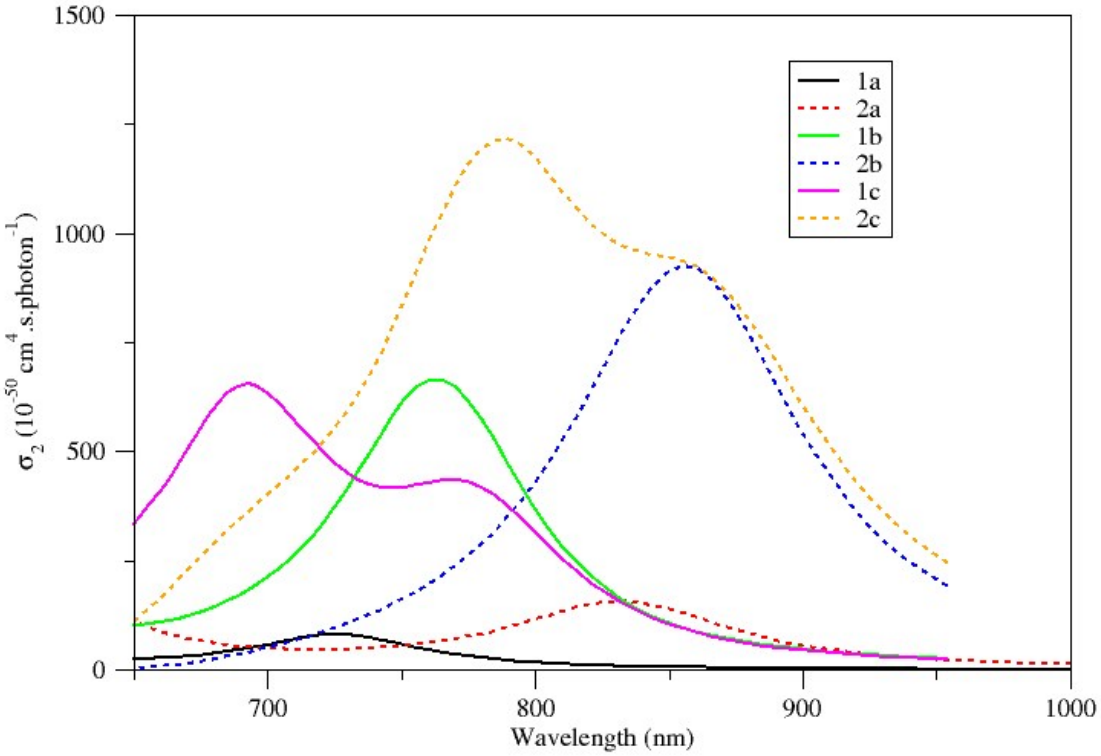

Figure S9. Computed 2PA spectra **1a-c** and **2a-c** in vacuum. See the main text for details on the computational protocol.

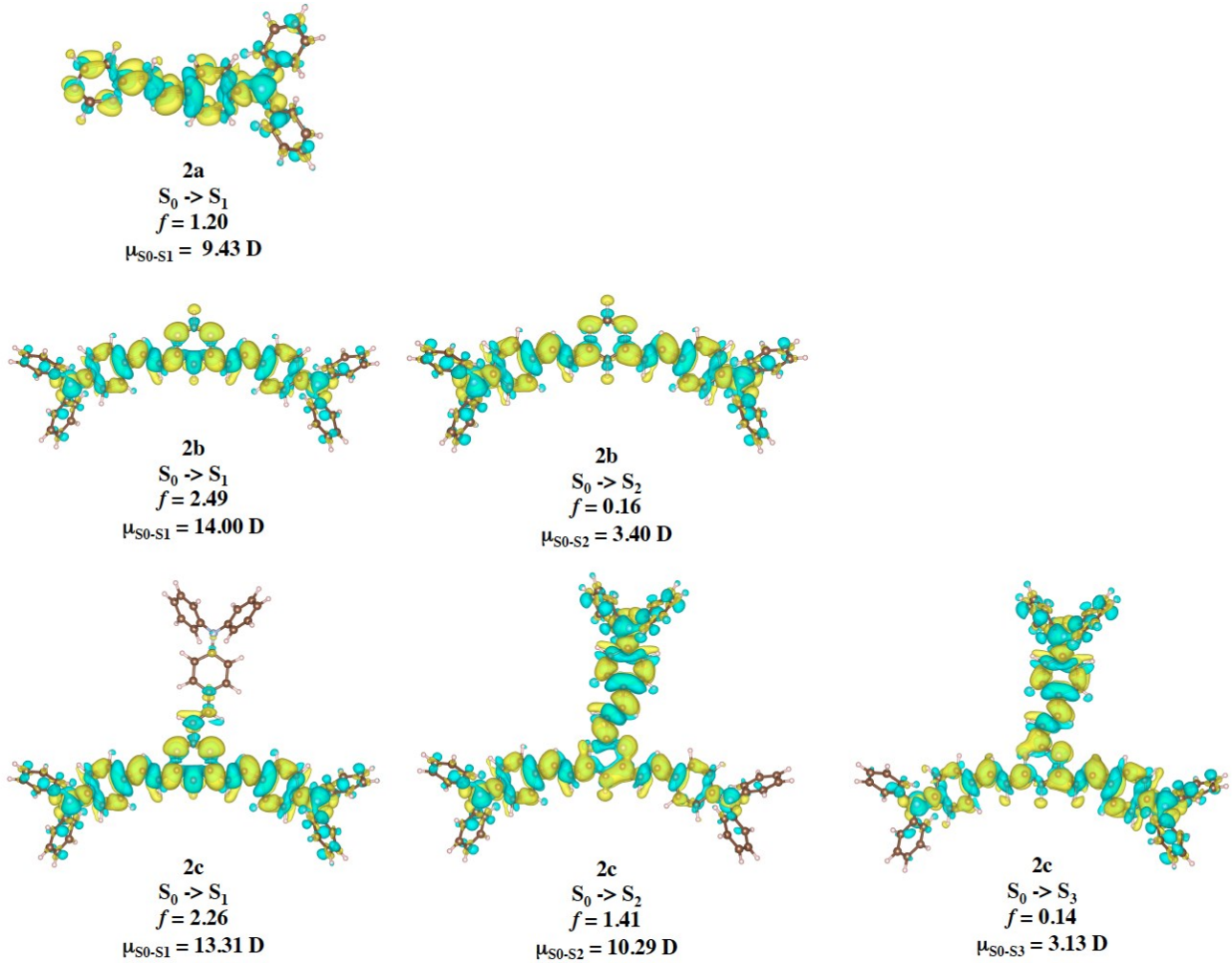

Figure S10. Additional transition densities of the lowest lying excited state in the **2a-c** series relevant to one and two photon absorption. *f* is the oscillator strength of the electronic transition and μ is the transition dipole moment value. See the main text for details on the computational protocol.

Additional computational details

Choice of the functional for excited-states properties:

Table S11 presents the theoretical optical properties obtained with two functionals: a global hybrid functional, PBE0, and a range-separated hybrid functional, CAM-B3LYP, that have been tested in this work as typical functional used for describing π-conjugated molecules excited-states [1]. For our series of donor acceptor molecules, charge-transfer transitions are widely present throughout the low-lying region of the spectrum, thus range-corrected

functionals like CAM-B3LYP are expected to perform better in general. More precisely, if CAM-B3LYP has already been proven to be one of the most accurate functional for excited-state geometry of extended π systems [2], Table S11 shows specifically in our cases that PBE0 predicts overestimated Stokes shift of the first excited-state for most of the compounds, while CAM-B3LYP returns shifts in agreement with the experimental spectra presented in Figure 2 (please note that the gas phase calculations are to be compared with spectra in non-polar solvents, like n-hexane or toluene). CAM-B3LYP results are thus only discussed in the main text of this work.

Basis set choice:

All results presented here are obtained with a relatively small 6-31G(d,p) basis set. This choice is motivated by the need of exploring excited-state geometries (and compute excited-state frequencies) for very large molecules at a reasonable computational cost. Increasing the basis set size showed only little improvement of the vertical transition energies when conducting test on the **1a**/**2a** molecule. For instance, upgrading the 6-31G(d,p) basis set to a 6-311+G(d,p) type do not change the nature of the CAM-B3LYP first electronic transition except for a red-shift ; 326 nm to 338 nm and 348 nm to 361 nm for **1a** and **2a,** respectively.

[1] D. Jacquemin, V. Wathelet, E. A. Perpète, and C. Adamo, Extensive TD-DFT Benchmark: Singlet-Excited States of Organic Molecules, *Journal of Chemical Theory and Computation,* **2009,** *5* (9), 2420-2435.

[2] C. A. Guido, D. Jacquemin, C. Adamo, and B. Mennucci, On the TD-DFT Accuracy in Determining Single and Double Bonds in Excited-State Structures of Organic Molecules, *The Journal of Physical Chemistry A,* **2010,** *114* (51), 13402-13410.

[3] Gaussian 03, Revision D.02, M. J. Frisch, G. W. Trucks, H. B. Schlegel, G. E. Scuseria, M. A. Robb, J. R. Cheeseman, J. A. Montgomery, Jr., T. Vreven, K. N. Kudin, J. C. Burant, J. M. Millam, S. S. Iyengar, J. Tomasi, V. Barone, B. Mennucci, M. Cossi, G. Scalmani, N. Rega, G. A. Petersson, H. Nakatsuji, M. Hada, M. Ehara, K. Toyota, R. Fukuda, J. Hasegawa, M. Ishida, T. Nakajima, Y. Honda, O. Kitao, H. Nakai, M. Klene, X. Li, J. E. Knox, H. P. Hratchian, J. B. Cross, V. Bakken, C. Adamo, J. Jaramillo, R. Gomperts, R. E. Stratmann, O. Yazyev, A. J. Austin, R. Cammi, C. Pomelli, J. W. Ochterski, P. Y. Ayala, K. Morokuma, G. A. Voth, P. Salvador, J. J. Dannenberg, V. G. Zakrzewski, S. Dapprich, A. D. Daniels, M. C. Strain, O. Farkas, D. K. Malick, A. D. Rabuck, K. Raghavachari, J. B. Foresman, J. V. Ortiz, Q. Cui, A. G. Baboul, S. Clifford, J. Cioslowski, B. B. Stefanov, G. Liu, A. Liashenko, P. Piskorz, I. Komaromi, R. L. Martin, D. J. Fox, T. Keith, M. A. Al-Laham, C. Y. Peng, A. Nanayakkara, M. Challacombe, P. M. W. Gill, B. Johnson, W. Chen, M. W. Wong, C. Gonzalez, and J. A. Pople, Gaussian, Inc., Wallingford CT, 2004.

i F. Terenziani, C. Katan, E. Badaeva, S. Tretiak and M. Blanchard-Desce, *Adv. Mater.*, **2008**, *20*, 4641-4678.